Martian corona: Nonthermal sources of hot heavy species

F. Cipriani, François Leblanc, Jean-Jacques Berthelier

Martian corona: Nonthermal sources of hot heavy species

F. Cipriani,[1] F. Leblanc,[2] and J. J. Berthelier[1]

Received 17 August 2006; revised 23 December 2006; accepted 30 March 2007; published 10 July 2007.

[1] We have studied the production of hot O and C atoms, and hot CO_2 and CO molecules in the Martian upper atmosphere and exosphere by dissociative recombination (DR) of O_2^+ and CO^+ ions, and sputtering of the atmosphere by incident O^+ pick-up ions. Production and collisional thermalization of the hot particles in the upper atmosphere are described by using a unique Monte Carlo test particle approach to simulate both nonthermal processes. Velocity distributions, atmospheric loss rates, and density profiles are derived for suprathermal O, C, CO, and CO_2 at low and high solar activity. At high solar activity the hot oxygen escape rate estimated from DR of O_2^+ is found to be less than two times the sputtering rate. Sputtering is found to efficiently populate the corona with molecular species such as CO and CO_2 at high solar activity and also to produce a carbon escape rate that is comparable to that derived from the major photochemical sources. Dissociation of CO_2 molecules by the impacting pick-up ions flux are found to produce about 50% of the sputtered exospheric oxygen density at high solar activity. Collisions of the background atmospheric gas with hot O atoms produced by DR of O_2^+ produce densities of hot CO_2 and CO molecules larger than 10^2 cm^{-3} for altitudes lower than 1000 km, at both high and low solar activity. Interestingly, the hot CO_2 density scale height is observed to be process dependent. The hot oxygen energy distributions associated with sputtering and DR near the exobase are also found to follow distinct decreasing energy laws. We suggest that the effects of the solar zenithal angle (SZA), crustal magnetic fields, and atmospheric tides on the ionospheric structure may produce exospheric signatures.

Citation: Cipriani, F., F. Leblanc, and J. J. Berthelier (2007), Martian corona: Nonthermal sources of hot heavy species, *J. Geophys. Res.*, *112*, E07001, doi:10.1029/2006JE002818.

1. Introduction

[2] Loss of volatiles from the Martian atmosphere is a topical subject, which aims at a better understanding of the water inventory at Mars [*Lammer et al.*, 2003; *Chassefière et al.*, 2006].The presence of hot neutral atomic species such as oxygen, carbon, and nitrogen is expected in the Martian upper atmosphere and exosphere from dissociative recombination (DR) of the main ionospheric ions O_2^+ [*Fox and Haćić*, 1997a, 1997b; *Kim et al.*, 1998; *Hodges*, 2000], N_2^+ [*Fox and Haćić*, 1997a, 1997b], CO^+ and CO_2^+ [*Fox and Haćić*, 1999; *Nagy et al.*, 2001; *Fox*, 2004], and from CO photodissociation [*Nagy et al.*, 2001]. O_2^+ and CO_2^+ ions have actually been detected by the Viking retarding potential analyzers [*Hanson et al.*, 1977] and by ASPERA3/MEX [*Carlsson et al.*, 2006]. Solar EUV ionizing radiation, solar wind electron impacts, and charge exchange reactions lead to the formation of exospheric ions [*Luhmann et al.*, 1992; *Modolo et al.*, 2005]. These ions can be accelerated antisunward by the motional electric field of the solar wind and be directly lost into space. Since the gyroradii of those ions around the interplanetary magnetic field lines is of the order of Mars radius, a fraction of them can impact the atmosphere and eject neutral atoms and molecules present near the exobase [*Luhmann and Kozyra*, 1991; *Johnson et al.*, 2000; *Leblanc and Johnson*, 2002]. The neutral energetic component of the Martian upper atmosphere and exosphere represents a critical measurement target to constrain the nonthermal escape rates and solar wind mass loading.

[3] Several authors have used numerical schemes to calculate the density profiles, velocity distributions, and escape fluxes of hot exospheric oxygen at Mars. *Hodges* [2000] used a test particle Monte Carlo procedure in which oxygen atoms created in DR of O_2^+ ions are followed through the Martian thermosphere and ionosphere and interact by collision with neutrals, ions, and solar photons. Using an extended version of this model, *Hodges* [2002] reported a range of calculated escape rates of hot oxygen over a solar cycle extending from 4.4×10^{25} to 1.8×10^{26} s^{-1} in the daytime ionosphere. *Hodges* [2002] also reported an escape rate higher by a factor of 6 using the upper limit models of *Fox* [1993] which include both daytime and nighttime ionospheres. *Kim et al.* [1998] used the vibrational distribution of O_2^+ ions calculated by *Fox and Haćić* [1997a, 1997b] associated with the branching ratios measured by *Kella et al.* [1997] to model the hot oxygen

[1]Centre d'Etude des Environnements Terrestres et Planétaires/IPSL, Saint-Maur, France.
[2]Service d'Aronomie du CNRS/IPSL, Verrières-Le-Buisson, France.

0148-0227/07/2006JE002818

production through DR reaction at high and low solar conditions. The resulting hemispheric escape rates (as corrected following the work of *Nagy et al.* [2001]) amounted to 3.4×10^{25} s^{-1} at low solar activity and to 8.5×10^{25} s^{-1} at high solar activity. *Krestyanikova and Shematovich* [2005] calculated the hot oxygen densities, mean energy, upward fluxes, and energy distributions in the thermosphere (100–300 km) for low, mean, and high solar activity conditions by using a stochastic (Monte Carlo type) approach [*Shematovich*, 2004] to describe the collision of the hot component with the background atmospheric gas. Hard sphere collisional cross sections and elastic and inelastic differential cross sections were employed and compared, yielding hemispheric escape fluxes varying, respectively, from 6.5×10^{23} and 6.5×10^{24} s^{-1} at low solar activity to 6.5×10^{24} and 1.1×10^{25} s^{-1} at high solar activity.

[4] In the present paper we use a coupled test particle Monte Carlo and Molecular Dynamic approach adapted from the work of *Leblanc and Johnson* [2002] to calculate the exospheric density profiles for the hot O, C, CO, and CO_2 neutral species between 270 and 6000 km, as well as their velocity distributions and escape rates. Those hot particles are created by nonthermal sources such as sputtering of the atmosphere by incident O^+ pick-up ions and dissociative recombination of O_2^+ and CO^+ ions. *Leblanc and Johnson* [2002] used such procedures in order to study the effect of a multispecies atmosphere on the sputtering yield. In their approach, as well as in ours, the motions of the hot particles are affected only by the Martian gravity field and by the collisions with the atmospheric background. The Molecular Dynamic model allows to simulate the collisions involving molecules and takes into account the vibrational excitation of the molecules and the energy partitioning between the fragments when a dissociation occurs. The adapted Monte Carlo and Molecular Dynamic methods are briefly reviewed in section 2, and the sputtering and photochemical processes simulation schemes are described. In section 3, densities and velocities distributions of the hot coronal atoms and molecules are compared when produced by both types of mechanism at low and high solar activities. We conclude in section 4.

2. Model Description

2.1. Monte Carlo and Molecular Dynamic Schemes

[5] In our model the upper atmosphere and exosphere are divided into collisional and noncollisional domains. The collisional domain extends from 110 km to an altitude of 400 km arbitrarily fixed above the theoretical exobase so that the transition from collisional to collisionless regimes is correctly described. This domain is divided into 30 cells in the radial direction with exponentially distributed altitudes allowing an approximate constant number of atmospheric particles per cell. The noncollisional domain extends from 400 up to 6000 km. In this domain the output cells are linearly spaced with a height of 100 km. In order to study the dependence of our outputs on the thermospheric and ionospheric conditions, we have used two sets of thermosphere/ionosphere models to carry out our calculations. The first set was taken from the work of *Kim et al.* [1998]. The low solar activity model of *Kim et al.* [1998] was derived from the O, CO_2, CO, and O_2^+ density profiles from Viking measurements obtained at a solar zenithal angle (SZA) of 44°. The electron temperature was derived from Viking measurements [*Hanson et al.*, 1977] and from the model calculation of *Rohrbaugh et al.* [1979]. The high solar activity model was developed from the Mars Thermospheric General Circulation Model of *Bougher and Shinagawa* [1998] describing the neutral atmosphere without dust (at latitude 2.5°N and LT = 1500, i.e., SZA near 44°). The second model is that from the work of *Krasnopolsky* [2002]. It solves the continuity equations for 11 neutrals (formed by reactions involving CO_2, N_2, Ar, H_2, and HD parent species) and for 18 ionic species (among which CO_2^+, O^+, CO^+, C^+, N_2^+, N^+, Ar^+, H_2^+, H^+, and He^+ primary ions) and was constrained by the deuterium and hydrogen observations using HST [*Krasnopolsky et al.*, 1998], FUSE [*Krasnopolsky and Feldman*, 2001], and Mariner 6 and Mariner 7 [*Anderson and Hord*, 1971]. The low solar activity conditions are similar to that encountered during the Viking measurement (T_∞ = 200 *K*), and the high solar activity conditions are chosen close to those encountered during Mariner 6 and Mariner 7 measurements (T_∞ = 350 *K*). The solar conditions of the work of *Kim et al.* [1998] and *Krasnopolsky* [2002] are therefore similar, except that the SZA is equal to 44 in the work of *Kim et al.* [1998] and 60° in the work of *Krasnopolsky* [2002].

[6] In the present study we have adapted the Monte Carlo procedure used in the work of *Leblanc and Johnson* [2002] to account for new photochemical sources and for a spherical atmosphere. In this procedure, test particles (hot atoms or molecules) are followed as they move under the influence of the Martian gravity field in a fixed atmospheric background. Weights W_i^c are associated to the test particles in the simulation depending on their species and on the cell in which they have been created; in a cell c, a number N_i of hot particles of the species i will be described by $N_i^c = \frac{N_i}{W_i^c}$ test particles each representing W_i^c atmospheric particles of species i.

[7] The numerical scheme is such that (1) new hot oxygen or carbon atoms are created through dissociative recombination (distributed throughout the collisional domain) or new neutralized incident O^+ pick-up ions are created at the upper limit of the collisional domain, (2) the hot particles are moved in the gravitational field during a time step Δt, (3) binary collisions between hot particles and background atmospheric particles are simulated at the positions of each hot particle, and (4) particles whose energy falls below a given fraction of the escape energy are removed. Accounting for the weight associated with each test particle, the distribution function for each species in the phase space can be approximated by a summation over the test particle number. In order to limit the simulation length, weight values are chosen as large as possible (typically 10^{24}). Moreover, in order to avoid statistical errors, the lowest to largest weight values for each species in all the domain have to be as close as possible. In the case of DR a difficulty arises from the fact that the production rates of hot oxygen from 140 km (peak) to 350 km (minimum) differ by 4 orders of magnitude. In the present approach, weight values have been distributed in order to ensure that the number of test particles produced by DR above the exobase (from 200 to 400 km) represents about 10% of the total number of test particles created per time

step. In the case of sputtering, weights are kept equal throughout the collisional domain and for each species.

[8] Collisions involving molecules are treated by using the molecular dynamic model introduced by *Johnson and Liu* [1998] and applied to the Martian atmosphere by *Leblanc and Johnson* [2002]. In such a model, the impact parameter and the molecule orientation are chosen randomly and the equation of motion of the atoms during the collision is integrated using a fourth-order Gear predictor corrector model [*Allen and Tildesley*, 1987]. Morse-type potentials discussed in the work of *Johnson and Liu* [1998] are used to describe C-O and O-O interactions inside CO_2 and CO molecules and allow to calculate the dissociation probabilities. A dissociation occurs when the distance between two atoms in the molecule becomes larger than the cutoff distance of the potential [*Johnson and Liu*, 1998]. A so-called universal potential (UP) [*Ziegler et al.*, 1985] is used to describe the interactions between incident and target particles (both can be single atoms or atoms in molecules). During a collision, molecules can either dissociate or become vibrationally excited. In this latter case, the internal energy is conserved between two successive collisions in our simulation, meaning that quenching cooling of the molecule through radiation are neglected. However, the loss of energy of the particles by electronic excitation or ionization of atoms and molecules in the atmosphere is also accounted for. If the relative energy of the colliding particles, one being a molecule, is smaller than a few electronvolts, collisions are treated in the hard sphere approximation.

[9] This approach to describe the collisions has several drawbacks, and in particular, an improvement of the interaction potential will be required in a future simulation [*Johnson and Liu*, 1998]. The Morse potentials could include a more complicated long-range interaction term, which would primarily affect the calculation near the dissociation threshold at low energies. The universal potential also neglects the weak long-range attractive force relevant in the energy range of the DR products, which can induce the occurrence of orbiting collisions that lead to an enhanced interaction time, and therefore increase the dissociation probability. Furthermore, as shown by *Kharchenko et al.* [2000] and noted by *Krestyanikova and Shematovich* [2005], the elastic scattering of suprathermal atoms on atomic oxygen in the 0–5 eV energy range is characterized by small scattering angles. This angular dependence of the differential cross section for elastic scattering in the low energy range emphasizes the necessity to improve the interaction potentials used.

[10] In this context, in order to understand in which way the use of the universal potential will influence the derived escape rates for hot oxygen, we have compared differential collision cross sections and energy transfer cross sections computed from the universal potential for O-O collisions in the energy range of the DR products, with differential collision cross sections and energy transfer rates calculated from exact quantum approaches as in the work of *Kharchenko et al.* [2000] and in the work of *Tully and Johnson* [2001]. This comparison showed us that the use of the universal potential led to an overestimation of the thermalization rate in our model due, on the one hand, to larger UP-based differential collision cross sections (by a mean factor of 2 compared to more accurate differential collision cross sections) and, on the other hand, larger UP-based energy transfer cross sections (by a mean factor of 1.3 for transferred energies lower than about 1 eV compared to more accurate energy transfer cross sections). As a consequence the escape rates obtained in the present paper, in the case of DR, can be seen as lower bounds of the escape rates values due to collisions of the thermal background with hot atoms in the energy range of the DR products.

2.2. Nonthermal Processes

2.2.1. Sputtering

[11] The solar wind interaction with the Martian atmosphere has been described by *Zhang et al.* [1993] at epoch 1, 2, and 4.5 Gyr after the beginning of the solar system, corresponding, respectively, to a solar EUV intensity equal to 6, 3, and 1 times the present EUV flux at solar minimum conditions. The thermospheric conditions for each of these epochs were calculated by *Zhang et al.* [1993], and in particular, the hot oxygen fluxes and densities produced from dissociative recombination of O_2^+ ions were evaluated. *Luhmann et al.* [1992] have used these densities to estimate the nonthermal atmospheric loss rates at these three epochs as well as the precipitating O^+ pick-up ions fluxes at the Martian exobase. These fluxes were calculated using a gas dynamic magnetic field model [*Spreiter and Stahara*, 1980] coupled to a test particle model. *Leblanc and Johnson* [2002] used this impacting flux to calculate the sputtering yield at different epochs and derived the related H_2O loss from a one-dimensional molecular atmosphere. Recently, new incident O^+ pick-up fluxes have been determined at low solar activity from the work of *Modolo et al.* [2004]. These authors developed a three-dimensional hybrid description of the solar wind interaction with Mars in which ions are treated kinetically and electrons are considered as a massless fluid. Such hybrid description is particularly relevant to take into account the kinetic effects essential in Mars' solar wind mass loading and when deriving the flux of incident pick-up ions [*Brecht*, 1997].

[12] In this paper, we use the pick-up ion flux calculated by *Modolo et al.* [2004] at low solar activity (dotted line in Figure 1) which corresponds to 5.9×10^{23} particles s^{-1} impacting the Martian exobase (to be compared to 5×10^{23} particles s^{-1} in the case of the work of *Luhmann et al.* [1992]). At high solar activity, we use a mean flux of 3.6×10^{25} s^{-1}, which is a linear extrapolation of the 1EUV and 3EUV fluxes obtained by *Luhmann et al.* [1992]. Because the pick-up ions are neutralized well above the exobase level by charge exchange [*Luhmann and Kozyra*, 1991], only collisions between neutral particles are considered in our model. However, this assumption may have to be considered further in a future study, since recent measurements of the solar wind and planetary plasma around Mars by ASPERA-3/Mars Express have shown that solar wind ions could penetrate down to ionospheric altitudes (270 km) on the Martian dayside [*Lundin et al.,* 2004]. The energy spectra of the impacting particles at high (dashed line) and low (dotted line) solar activities used in our simulation, as well as the one from the work of *Luhmann et al.* [1992] (solid line), are displayed in Figure 1.

[13] In our simulation, the neutrals impacting the Martian exobase have energies between 50 eV (a threshold arbitrarily fixed since, below such an energy, an O particle

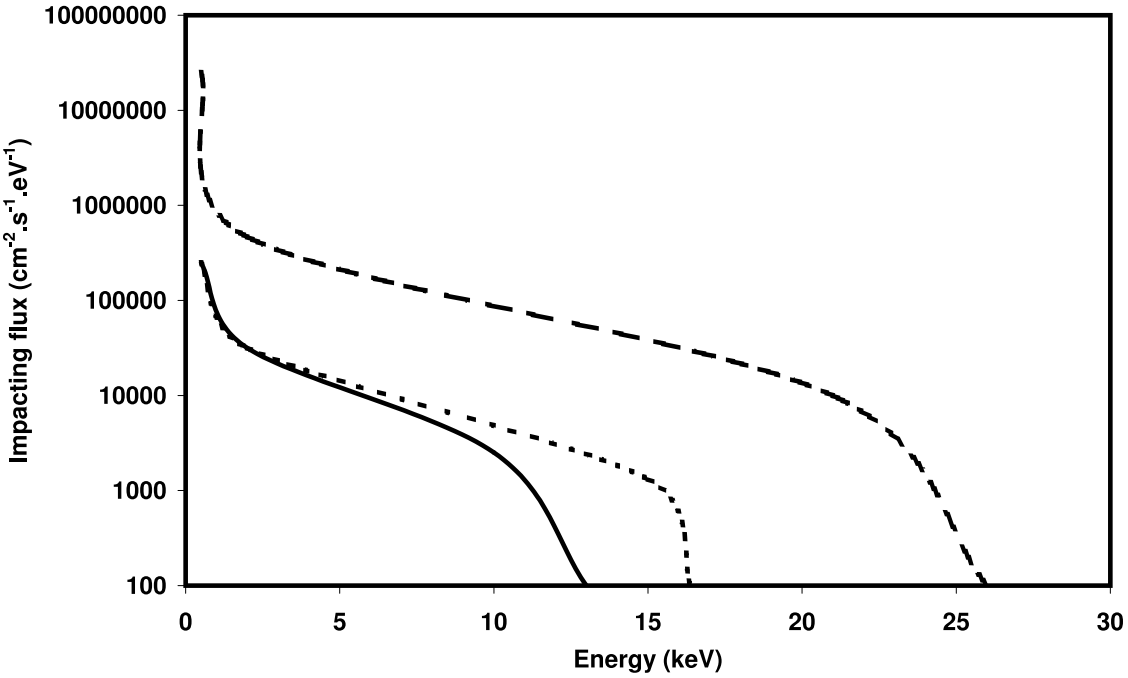

Figure 1. Energy spectra of the incident O^+ pick-up ion fluxes as calculated by *Luhmann et al.* [1992] (solid line), and by *Modolo et al.* [2004] (dotted line), and used in the present study at high solar activity (dashed line).

is supposed to have a negligible efficiency in ejecting atmospheric particles [*Johnson et al.*, 2000]) and 26 keV (cf. Figure 1). Incident particles crossing the upper limit of the collisional domain at 400 km are followed until they

[14] ● Reach the bottom limit at 110 km and are considered as thermalized by the dense atmospheric gas (cannot produce any recoil particle that will cross the exobase) or

[15] ● Lose their energy in a collision cascade within the upper atmosphere up to the moment when this energy becomes smaller than a given fraction of the escape energy (typically 0.04 eV for oxygen at 270 km) or

[16] ● Are ejected from the collisional domain and escape or

[17] ● Cross the upper limit of the calculation domain, located at two Martian radii.

2.2.2. Photochemical Reactions

2.2.2.1. O_2^+ Dissociative Recombination

[18] The dissociative recombination of O_2^+ with electrons leads to the creation of a corona of hot O atoms at Mars and Venus (see for instance *Fox and Hać* [1997a, 1997b] and *Hodges* [2000]). Dissociative recombination exothermicity strongly depends on the vibrational state of the O_2^+ molecule, as one vibrational quantum adds 0.24 eV to the released energy. Several authors [*Fox and Hać*, 1997a, 1997b; *Kim et al.*, 1998; *Hodges*, 2000] have used measurements of branching ratio for O_2^+ in the ground vibrational state from the work of *Kella et al.* [1997] in order to simulate the dissociative recombination. *Fox and Hać* [1997a, 1997b] have determined the vibrational distribution of the O_2^+ ions at the Martian exobase from the Monte Carlo simulation of $O^+ + CO_2 \rightarrow O_2^+ + CO$ and $CO_2^+ + O \rightarrow O_2^+ + CO$ reactions, as well as reaction of relaxation quenching of the vibrational states of O_2^+. *Kabin and Shizgal* [2002] computed nascent velocities of hot ^{16}O and ^{18}O using an analytical approach and obtained a good agreement with the work of *Fox and Hać* [1997a, 1997b], assuming the same vibrational levels distributions for O_2^+ in the Martian atmosphere.

[19] Modeling studies of this reaction in planetary atmospheres mainly suffer from the fact that the vibrational distribution of O_2^+ in the ionosphere is unknown on the one hand and that, on the other hand, measured rates and branching ratios in storage ring experiments result from a mixture of vibrationally excited O_2^+ atoms. A recent study [*Petrignani et al.*, 2005] reported measurements of vibrationally resolved branching ratios in the DR of O_2^+ for the first three vibrational levels of O_2^+. Those latter results will be accounted for in the next implementation of our model.

[20] In the present study we have used measurements of *Peverall et al.* [2001] of dissociative recombination branching ratios, when O_2^+ ions are produced in their vibrational ground state, as a function of the relative electron kinetic energy, up to 3000 K. Those measurements allowed us to introduce an altitude dependence of the branching ratio, hence an altitude dependence of the velocity distribution of the hot O atoms produced by DR of O_2^+, by using the ionospheric temperature profiles from the work of *Kim et al.* [1998] or *Krasnopolsky* [2002]. Values of the branching ratios are interpolated from the tabulated values given in the work of *Peverall et al.* [2001] as a function of the computed relative energy of the ions and electrons (see Figure 2). Nascent velocities of the hot O atoms are then derived from Gaussian distributions centered on the mean values of the DR channels taken from the work of *Kella et al.* [1997], for which a mean FWHM of 0.5 eV is assumed. From the measurements of *Kella et al.* [1997], when O_2^+ is not

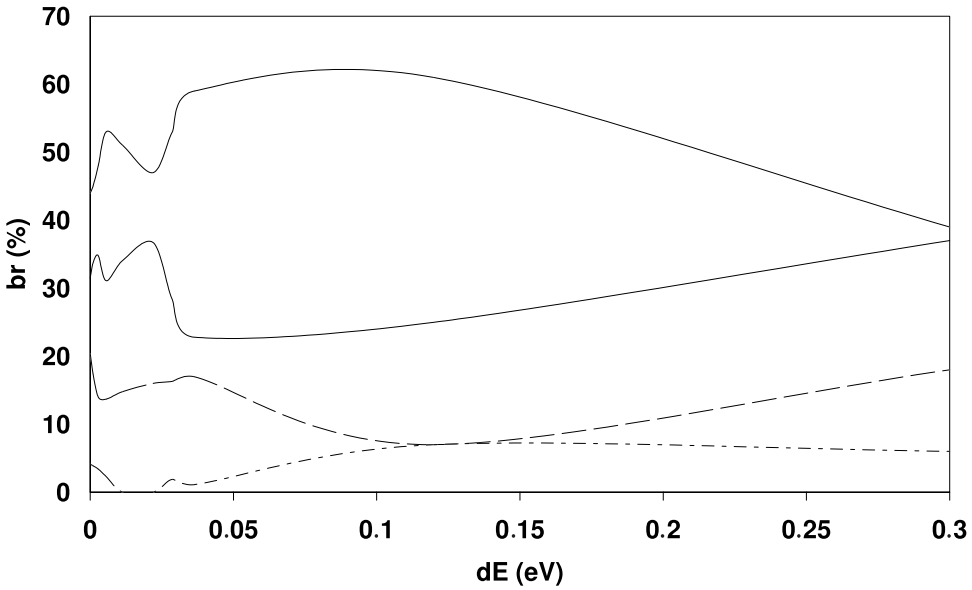

Figure 2. Branching ratios (br) for DR of O_2^+ as a function of the translational relative energy between the electrons and ions (dE). Values per channel given in the work of *Peverall et al.* [2001] have been linearly interpolated as follows: C1 channel, dashed line; C2 channel, dotted line; C3 channel, solid line; C4 channel, dashed dotted line.

vibrationally excited ($\nu^i = 0$), the following branching ratios and exothermicities were associated with the dissociation channels C1 to C5 (values of the ratios are given in brackets):

$$\begin{aligned} O_2^+ + e^- &\rightarrow O(^3P) + O(^3P) + 6.95\ \text{eV}(0.22)(\text{C1}) \\ &\rightarrow O(^1D) + O(^3P) + 4.99\ \text{eV}(0.42)(\text{C2}) \\ &\rightarrow O(^1D) + O(^1D) + 3.02\ \text{eV}(0.31)(\text{C3}) \\ &\rightarrow O(^1D) + O(^1S) + 0.80\ \text{eV}(0.05)(\text{C4}) \\ &\rightarrow O(^3P) + O(^1S) + 2.77\ \text{eV}(< 0.01)(\text{C5}) \end{aligned} \quad (1)$$

[21] Since the exothermicity of the reaction strongly depends on the vibrational distribution of O_2^+ ions, we also carried out comparative simulations in which we account for the distribution of the nascent velocities of the hot oxygen atoms calculated by *Fox and Hać* [1997a, 1997b] and *Kabin and Shizgal* [2002] at the Martian exobase. No significant differences in the derived exospheric densities have been observed between those simulations. However, an oxygen escape rate enhancement of about 30% was obtained in the simulation accounting for the vibrational energy distribution of O_2^+. In the following, we show the results derived from the approach accounting for the vibrational distribution of O_2^+ ions, which has been commonly used by other authors [see, e.g., *Kim et al.*, 1998].

[22] The DR production rate considered in our simulation [see equation (2)] is the widely accepted rate measured by *Mehr and Biondi* [1969] and is in excellent agreement with recent measurements for O_2^+ in its vibrational ground state [*Sheehan and St-Maurice*, 2004].

$$\begin{aligned} \alpha = 1.95 \times 10^{-7}(300/T_e)^{0.7}\text{cm}^3\ \text{s}^{-1}, \quad 300\,\text{K} \le T_e \le 1200\,\text{K}, \\ 0.75 \times 10^{-7}(1200/T_e)^{0.56}\text{cm}^3\ \text{s}^{-1}, \quad 1200\,\text{K} \le T_e \le 5000\,\text{K}. \end{aligned} \quad (2)$$

where T_e is the electron temperature. The velocity vectors of the hot atoms produced in the dissociative recombination process are then assumed to be isotropically distributed.

2.2.2.2. CO^+ Dissociative Recombination

[23] The escape of the atomic carbon plays an important role in the CO_2 planetary inventory. The main expected photochemical escape sources are photodissociation of CO, dissociative recombination of CO^+ reactions, and electron impact dissociation of CO [*Fox*, 2004]. CO_2^+ dissociative recombination is also responsible for the major part of the thermospheric density of atomic carbon.

[24] In the present study, escape rates and densities are calculated only for hot carbon created by dissociative recombination of CO^+. Although this is not the major escape source for hot atomic carbon, this source of hot C atoms can interestingly be compared to the carbon loss induced by sputtering (see sections 3.1 and 3.2). The energetic channels associated with the dissociative recombination of CO^+ are the following [see, e.g., *Nagy et al.*, 2001]:

$$\begin{aligned} CO^+ + e^- &\rightarrow C(^3P) + O(^3P) + 2.90\,\text{eV}(\text{C1}) \\ &\rightarrow C(^1D) + O(^3P) + 1.64\,\text{eV}(\text{C2}) \\ &\rightarrow C(^3P) + O(^1D) + 0.94\,\text{eV}(\text{C3}) \\ &\rightarrow C(^1S) + O(^3P) + 0.22\,\text{eV}(\text{C4}) \\ &\rightarrow C(^1D) + O(^1D) + 0.33\,\text{eV}(\text{C5}) \end{aligned} \quad (3)$$

The corresponding branching ratios for channels (C1) to (C5), as measured by *Rosen et al.* [1998], are, respectively, 0.761, 0.145, 0.094, and 0.0 at 0 eV relative energy (in this case, the C5 endothermic channel is not possible) and become 0.53, 0.34, 0.08, 0.0, and 0.05 at 0.4 eV relative

energy. The relative energy of the CO^+ ions and the electrons is computed in our simulation as a function of altitude from the temperature profiles. The branching ratios are then interpolated between the 0 and 0.4 eV values given above. The rate coefficient we have used is that measured by *Rosen et al.* [1998]:

$$\alpha = 2.75 \times 10^{-7}(300/T_e)^{0.55}\text{cm}^3\ \text{s}^{-1} \quad (4)$$

where T_e is the electron temperature.

3. Results and Discussion

3.1. Hot Coronal Densities

[25] The hot O component of the Martian corona has been described earlier either as created by DR of O_2^+ [*Kim et al.*, 1998; *Hodges*, 2000; *Krestyanikova and Shematovich*, 2005] or created by the pick-up ion sputtering of the atmosphere [*Johnson and Luhmann*, 1998; *Leblanc and Johnson*, 2001]. Here we use the same numerical scheme to simulate both the DR and sputtering processes and compare their respective influence on the coronal structure. Figure 3 provides the calculated density profiles for O, C, CO_2, and CO resulting from those processes as a function of the altitude. In this case the thermosphere and ionosphere models are those from the work of *Kim et al.* [1998] (section 2.1).

[26] The hot oxygen densities calculated at low solar activity are plotted in Figure 3a. Dissociative recombination of O_2^+ is clearly seen to dominate the production of hot coronal oxygen, the DR (black solid line) to sputtered (black dashed line) oxygen density ratio being on the order of 100 at 1000 km. The density profile of hot oxygen calculated here (black solid line) is very close to that calculated by *Hodges* [2000] in the Mars-L case (line with triangles). The hot O density from DR of O_2^+ plotted on Figure 3a is a factor of 2 smaller than that obtained in the work of *Kim et al.* [1998] (line with squares). The approach used by *Kim et al.* [1998] was based on a two-stream model calculation [*Nagy and Banks*, 1970] yielding the hot oxygen fluxes as a function of altitude and energy, below the exobase. The isotropic distribution functions at the exobase were then used as inputs into an exosphere model based on Liouville's theorem [*Schunk and Nagy*, 2000]. Methodological differences may therefore account for the observed discrepancies. However, we found a ratio of the hot O densities calculated at high and low solar activities of the order of two, which is consistent with the ratio obtained by *Kim et al.* [1998].

[27] The large difference observed at solar minimum between the hot O densities produced by sputtering and the hot O densities produced by dissociative recombination is largely reduced at solar maximum (Figure 3b). *Johnson and Luhmann* [1998] estimated that the ratio of the hot O density produced by sputtering to the hot O density produced by DR at an equivalent 2EUV period (solar maximum activity) most probably belongs to the range 0.25–0.5. Our results clearly indicate a ratio larger than 0.5 for altitudes below 1000 km. This indicates that sputtering is an important source of hot exospheric oxygen at high solar activity. Moreover, as can be seen on (Figure 3d), sputtering significantly populates the exosphere with hot molecular species as CO and CO_2 at high solar activity, especially at altitudes lower than 1000 km. Because of the increase of the incident pick-up ions flux between low and high solar activities (from 5.9×10^{23} to 3.6×10^{25} O^+ ions/s), the densities of hot O, CO_2, CO, and C created by sputtering (Figures 3b and 3d) increase in the same proportion.

[28] The energy transferred in the collisions of the hot O atoms produced by DR of O_2^+ with the atmospheric background remarkably appears to create a significant amount of exospheric CO and CO_2 molecules at both high and low solar activity, especially below 1000 km, where we observe densities higher than 10^2 cm^{-3}. The density of those hot molecules at such altitudes is also seen as nearly independent on the solar activity. Since the ionic peak position is roughly at the same altitude at both low and high solar activity [*Kim et al.*, 1998], the hot particles which have an upward velocity vector cross an atmospheric column density above the ionic peak which is larger at high solar activity than it is at low solar activity. Therefore the hot exospheric CO and CO_2 produced by collisions with the hot O atoms created by DR at high solar activity will make a larger number of collision before reaching the exobase than at low solar activity. In the end, the scale heights of the hot CO_2 density profiles in Figures 3b and 3d are seen as dependent on the creation process, at both low and high solar activity. As a consequence, an in situ measurement of this scale height should provide clues to identify the origin of the exospheric CO_2.

[29] From Figure 3b it can be noticed that, at high solar activity, sputtering and DR of CO^+ ions appear as fairly comparable sources of hot atomic carbon in the exosphere since the hot C density due to the DR of CO^+ ions is comparable to the hot carbon density due to the sputtering of the thermosphere.

[30] The dependency of our results on the atmospheric model has also been tested by comparing these results to similar results but using the self-consistent thermosphere/ionosphere one-dimensional model from the work of *Krasnopolsky* [2002]. As can be seen on Figure 4, the hot O density profile produced by DR and obtained using this latter model for low solar activity (solid line with diamonds) is up to five times smaller than the densities obtained using the model of *Kim et al.* [1998] (solid line). This discrepancy is reduced by a factor of 2 at high solar activity (see the dashed-dotted and dashed lines). The observed discrepancies can be mainly related to the variation of the ionospheric peak density, following different SZA values.

[31] The dependence on the ionosphere was tested by carrying out a set of calculations using the model of *Krasnopolsky* [2002] in which the ionosphere is replaced by that of *Kim et al.* [1998]. The resulting density of hot oxygen at low solar activity is the dotted line plotted on Figure 4 and is very close to the result obtained with the model from the work of *Kim et al.* [1998]. On the contrary, at high solar activity, the ionospheric models of *Kim et al.* [1998] and *Krasnopolsky* [2002] are much closer than at low solar activity, as can be seen, respectively, from Figures 1a and 3b of those works, and can not explain the observed factor of 2 between the dashed-dotted and dashed lines by themselves. In this case, however, the thermosphere of the work of *Krasnopolsky* [2002] also clearly contributes, since it appear as significantly denser than that from the work of *Kim et al.* [1998]. This, in the end, provides an explanation for the larger hot O exospheric density observed when we

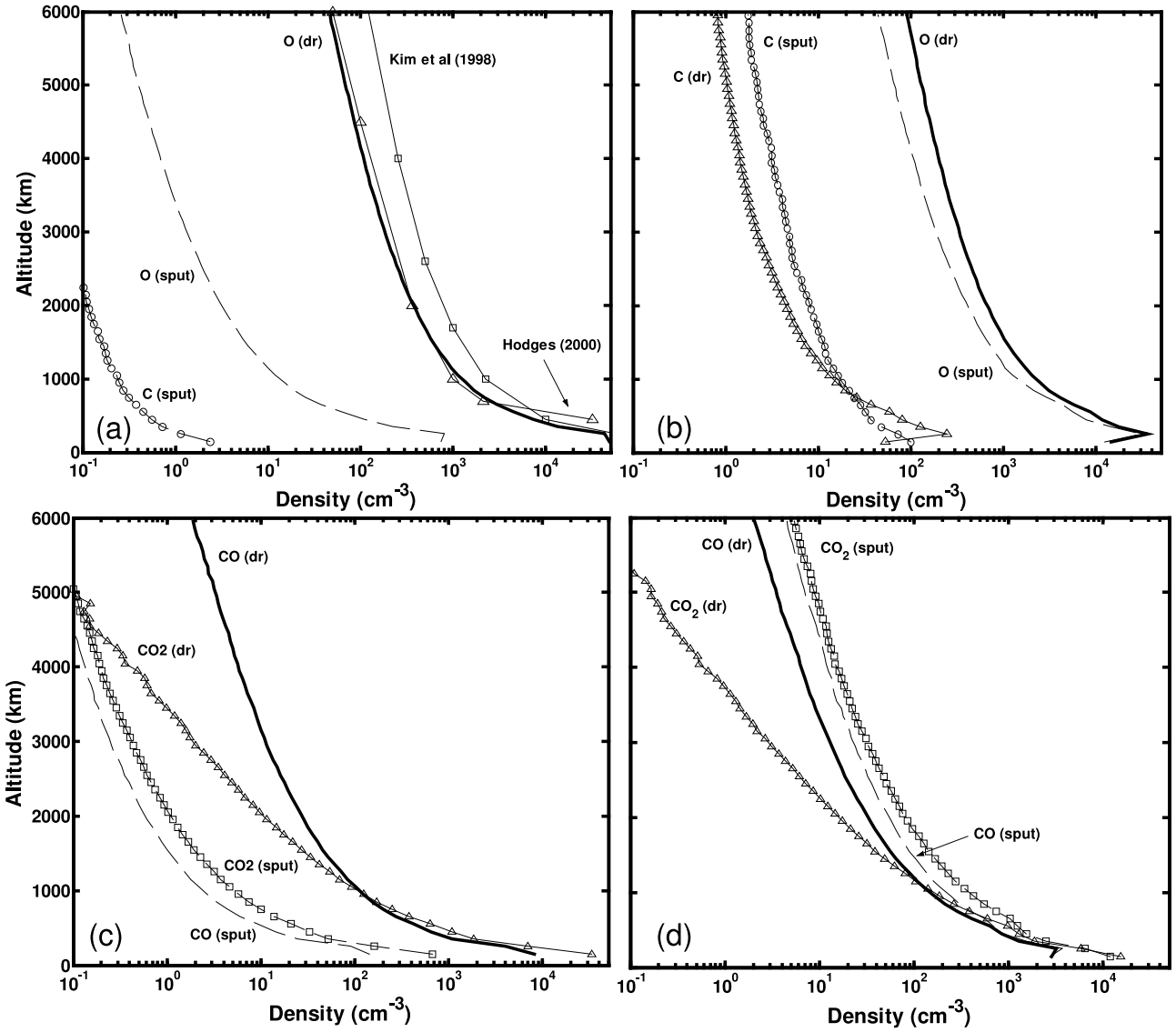

Figure 3. Density profiles for hot O, CO_2, CO, and C for low (Figures 3a and 3c) and high (Figures 3b and 3d) solar activities. (a) Oxygen produced in dissociative recombination of O_2^+ ions (lines labeled dr) and Sputtering of the atmosphere by O^+ pick-up ions (lines labeled sput). Comparisons can be done between sputtered O (dashed), DR-produced O (solid), O density in the work of *Kim et al.* [1998] (squares), O density from the work of *Hodges* [2000] (triangles). (b) Oxygen and carbon produced in dissociative recombination of O_2^+ and CO^+ ions and sputtering of the atmosphere by O^+ pick-up ions: sputtered O (dashed), sputtered C (dashed-circles), DR-produced O (solid), DR-produced C (triangles). No results are available at high solar activity from the work of *Hodges* [2000]. (c) Density profiles for CO_2, CO, and C resulting from the same processes. Square and dashed lines, respectively, apply to CO_2 and CO created by sputtering, whereas solid and triangle lines apply, respectively, to CO and CO_2 created in collisions with hot oxygen produced by DR of O_2^+ ions. (d) Same legend as Figure 3c.

base our calculations on the model from the work of *Kim et al.* [1998]. This dependence of the ionosphere on the SZA, particularly significant at low solar activity in the above calculation, is well known, and a decrease of the electron density with SZA has been observed by the Viking radio occultation experiment [*Zhang et al.*, 1990], showing that the ion densities are small on the nightside. Those results hence illustrate the large spatial variations of the hot O production by DR that can be expected as a function of the solar zenithal angle. It shows that the maximum of the production rate of the DR process may be expected near the subsolar region. *Krymskii et al.* [2003] derived longitudinal variations of the electron peak density in the northern hemisphere from Mars Global Surveyor radio science data and found a density enhancement correlated with the location of a large-scale crustal magnetic anomaly between 67° and 80° of latitude. This density enhancement also led to an electronic temperature enhancement consistent with trapped magnetospheric electrons. *Bougher et al.* [2004] observed repeatable density peak height variations at high

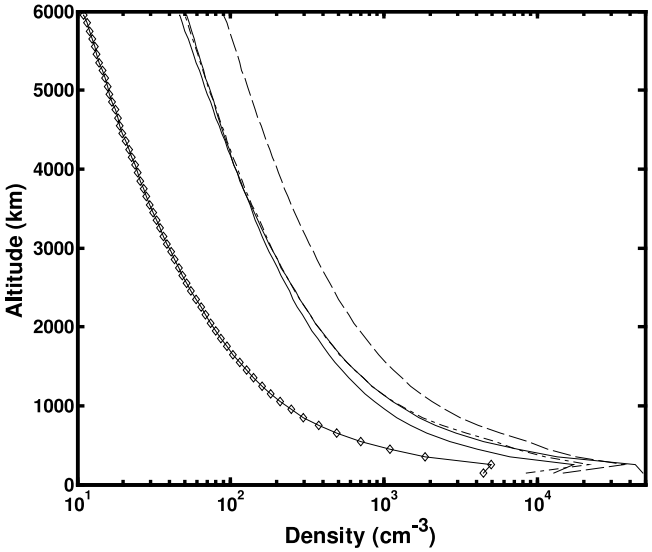

Figure 4. Influence of *Kim et al.* [1998] and *Krasnopolsky* [2002] thermospheric/ionospheric models on the hot O density created by dissociative recombination reactions. Line with diamonds, Krasnopolsky low solar activity. Dashed dotted line, Krasnopolsky high solar activity. Solid line, Kim low solar activity. Dashed line, Kim high solar activity. Dotted line, Krasnopolsky thermosphere with Kim ionosphere at low solar activity.

latitudes (65°–78°N) and during aphelion conditions as a function of longitude over 2 Martian years. Those variations were seen to result from upward-propagating nonmigrating tides generated by the interaction of migrating tides with the Martian topography. Those observations together with our predictions of the influence of the ionospheric content have direct implication on the exospheric structure. Since the DR of O_2^+ rate depends on the electron density and temperature, the longitudinal variations of those parameters can lead to variations of the related hot O density in the exosphere. The altitude of the ionospheric peak will also play an important role, as we have seen in the case of CO_2 and CO, since its position in the thermosphere determines the densities of the heavy particles in the exosphere. The study of the net effect of those parameters on the hot O production from DR of O_2^+, however, requires further modeling. We hence notice that the crustal magnetic field which plays a role in the ionospheric content (as shown by *Krymskii et al.* [2003]) may have a signature in the exospheric density produced by DR.

[32] In the case of sputtering, a recent three-dimensional simulation based on a hybrid description of the solar wind interaction with Mars [*Modolo et al.*, 2004] describes the flux of impacting energetic oxygen atoms as strongly asymmetric around Mars and impinging preferentially on the side of the planet opposite to the solar wind convection electric field direction. The maximum of the sputtered neutrals should therefore appear as located near the terminator on the evening or morning side, depending on the IMF orientation and intensity, as well as on the ionizing flux intensity. The ejection and intensity peak region for sputtering will therefore vary as a function of the direction of the convection electric field of the solar wind, whereas DR process should be mostly dependent on the SZA.

[33] The effect of the molecular dissociations on the sputtering efficiency of the incident O^+ pick-up ions has been investigated in the work of *Leblanc and Johnson* [2002]. In particular, these authors have shown that molecular dissociations do not enhance the sputtering yield and the corresponding escape rates of the atmospheric components. In the present study, we compare the hot oxygen exospheric densities obtained through sputtering at high solar activity when those dissociations are considered (case 1) and when they are not (case 2) by using the atmospheric model of *Kim et al.* [1998]. We confirm that, in case 1, dissociations of molecules do not enhance the escape rates. Comparing cases 1 and 2 we observed that the hot oxygen exospheric density is enhanced by a factor of 2 when the molecular dissociations are included, meaning that about 50% of the hot oxygen atoms formed by sputtering comes from the dissociation of a CO_2 molecule or a CO molecule in those conditions. The molecular dissociation peak was found at an altitude near 150 km in the thermosphere. We also computed an associated average production rate of oxygen from dissociated molecules of 1.3×10^7 cm^{-3} s^{-1} at high solar activity, those atoms being produced with a mean energy of 44 eV. The position of this molecular dissociation peak corresponds to a fraction of about 55% of the initial energy of the impacting flux deposited in the thermosphere above 150 km in altitude.

3.2. Escape Rates

[34] Using the atmospheric background from the work of *Kim et al.* [1998], escape rates integrated over one hemisphere have been derived for the DR of O_2^+ and DR of CO^+, as well as for sputtering, and are summarized in Table 1. In the case of the DR of O_2^+, results obtained with the atmospheric background from the work of *Krasnopolsky* [2002] are also given.

[35] In the case of dissociative recombination, at low solar activity, our results for the oxygen escape rate (2.1×10^{25} s^{-1}) is in reasonable agreement (within a factor of 2) with that from the work of *Kim et al.* [1998] (3.4×10^{25} s^{-1}) and with that from the work of *Hodges* [2002] (4.4×10^{25} s^{-1}). *Hodges* [2000] found a dayside escape rate for oxygen equal to 2.8×10^{25} s^{-1}, which is also of the same order as the rate we have computed. We find an escape rate of a factor of 3.6 lower than result in the work of *Hodges* [2002] at high solar activity (1.8×10^{26} s^{-1}). The model of *Hodges* [2002] accounts for the collisional quenching and excitation transfer of O(^{1}D) and O(^{1}S), using cross sections adopted from the work of *Shematovich et al.* [1999] and the high and low solar activity atmospheric models in the work of *Kim et al.* [1998]. The observed discrepancies between our model and that from the work of *Hodges* [2002] are, however, difficult to explain because *Hodges* [2002] lacked a detailed description of the parameters used in his model. The hemispheric escape rate in the work of *Krestyanikova and Shematovich* [2005] at solar minimum (6.5×10^{24} s^{-1}) is roughly four to five times lower than ours (calculated with the atmosphere in the work of *Kim et al.* [1998]). It is slightly larger than the rate (5.5×10^{24} s^{-1}) we have calculated using the atmosphere in the work of *Krasnopolsky* [2002]. At solar maximum our escape rate is lower by a factor of 2 using the atmosphere in the work of *Kim et al.* [1998] compared with the

Table 1. Comparative Escape Rates for Dissociative Recombination and Sputtering Processes

Models	Low Solar Activity (s^{-1})	High Solar Activity (s^{-1})
Dissociative recombination of O_2^+ (this paper)		
O (Kim atmosphere)	2.1×10^{25}	5×10^{25}
CO (Kim atmosphere)[a]	5×10^{22}	5.8×10^{22}
O (Krasnopolsky atmosphere)	5.5×10^{24}	2.6×10^{25}
O [*Hodges*, 2002][b]	4.4×10^{25}	1.8×10^{26}
O [*Kim et al.*, 1998] (corrected values)[c]	3.4×10^{25}	8.5×10^{25}
O [*Krestyanikova and Shematovich*, 2005][d]	6.5×10^{24}	1.1×10^{26}
Dissociative recombination of CO^+ (this paper)		
C (Kim atmosphere)	4.6×10^{20}	4.1×10^{22}
Sputtering (this paper)		
O	4.9×10^{23}	3.7×10^{25}
CO_2	2.3×10^{22}	1.8×10^{24}
CO	3.5×10^{22}	2.2×10^{24}
C	8.3×10^{22}	5×10^{24}
Sputtering [*Leblanc and Johnson*, 2002][e]		
O	3.4×10^{23}	4.1×10^{25}
CO_2	4.8×10^{22}	2.8×10^{24}
CO	3.6×10^{22}	2.4×10^{24}
C	8.8×10^{22}	7.5×10^{24}

[a]Escape of CO is induced by collisions with hot O created in dissociative recombination of O_2^+ ions. Escape of CO_2 through that channel is not observed.

[b]*Hodges* [2002] accounted for collisional quenching and excitation transfer of $O(^1D)$ and $O(^1S)$ in a day only ionosphere case (Mars-L case of the model of *Hodges* [2000]), using solar minimum and maximum thermospheric and ionospheric entries of *Kim et al.* [1998].

[c][*Kim et al.,* 1998] values are corrected by a factor of 6.5 [*Nagy et al.*, 2001] to account for the dayside hemispheric escape rate.

[d]Elastic and Inelastic channels for O-O and O-CO_2 collisions model B case of *Krestyanikova and Shematovich* [2005], integrated over one hemisphere.

[e]Solar maximum values are derived from the mean (1EUV + 3EUV) escape rates in the work of *Leblanc and Johnson* [2002].

escape rate calculated by *Krestyanikova and Shematovich* [2005]. Using the atmosphere in the work of *Krasnopolsky* [2002] it is lower by a factor of 4. Hence our escape rate remains significantly lower than the result in the work of *Krestyanikova and Shematovich* [2005].

[36] Model B of *Krestyanikova and Shematovich* [2005] takes into account the elastic and inelastic channels for O-O and O-CO_2 collisions and is based on the atmosphere in the work of *Krasnopolsky* [2002]. Dissociative recombination was treated in the work of *Krestyanikova and Shematovich* [2005] with the branching ratios from the work of *Kella et al.* [1997], and the production rate was calculated following the works of *Mehr and Biondi* [1969] and *Alge et al.* [1983]. The nascent velocity distribution of the dissociative recombination products was derived from the analytical formulation in the work of *Kabin and Shizgal* [2002]. The elastic differential collision cross sections used in their work lead to large probabilities of scattering with small angles for the typical collision energies of the DR products. In our case, as stated in section 2.1, the collision treatment is simplified to the use of a universal potential for this energy range. In this case, we have seen that the corresponding differential cross sections and energy transfer cross sections were larger than in the work of *Krestyanikova and Shematovich* [2005]. As a consequence, the thermalization rate of the hot O atoms through collisions with the background gas in the model of *Krestyanikova and Shematovich* [2005] is probably lower than in our model which hence result in a larger oxygen escape rate than in our case. This effect is much more pronounced at high solar activity than it is at low solar activity because the column density above the ionospheric peak is slightly larger (about 1.4×10^{16} against 10^{16} cm^{-2} at low solar activity). This result once again illustrates that the relative location in the thermosphere of the ionospheric peak greatly influences the atmospheric escape rates. From that point of view a measurement of the escape fluxes at Mars could advantageously be correlated with the simultaneous sounding of the ionospheric structure.

[37] At solar maximum we find that the sputtered-induced hot oxygen escape rate is 3.7×10^{25} s^{-1}, which represents approximately 0.75 times the DR-induced rate.

[38] We have computed a weak escape rate of CO of 5×10^{22} s^{-1} produced by the collisions of the atmospheric background with hot O produced by the DR of O_2^+. The corresponding escape flux would lead to an integrated CO loss of roughly 5.5×10^{39} molecules over 3.5 Gyr, if we consider that CO loss through this process is only weakly dependent on the solar activity as suggested by Table 1. Such loss is small compared to the 6.5×10^{41} molecules estimated in the case of the sputtering by *Leblanc and Johnson* [2002]. The computed escape rate of CO due to collisions of the atmospheric background with hot O produced by the DR of O_2^+ is of the same order than the escape rate of CO due to the sputtering at solar minimum activity (see Table 1). We observe that the corresponding escape rate of carbon (that is in the CO form) is negligible compared to the dayside escape rate of carbon (in the C form) resulting from CO photodissociation and dissociative recombination of CO^+, which has been estimated at low solar activity by *Nagy et al.* [2001] and *Fox and Bakalian* [2001], and amounts to 4×10^{23} s^{-1}. It is, however, far larger than the carbon loss (in the C form) due to the DR of CO^+ that we have computed (4.6×10^{20} s^{-1}). At high solar activity, the escape rate of atomic carbon (in the C form) that we have computed in the case of sputtering (5×10^{24} s^{-1}) is clearly comparable to the escape rate due to photochemistry estimated by *Nagy et al.* [2001], which equals 6.4×10^{24} s^{-1}, or to the escape rate due to photochemistry estimated by *Fox and Bakalian* [2001]. We find that the escape rate of carbon in all forms (C, CO, and CO_2) due to sputtering at high solar activity is 9×10^{24} s^{-1}. Therefore sputtering mechanism might be a major source of carbon escape in conditions of high solar activity. The arrangement of the density profiles of C, CO, and CO_2 in Figures 3c and 3d suggests that the flux of atomic carbon crossing the exobase is lower than the escaping flux of atomic carbon, whereas, in the case of the heavy species CO_2 and CO, the flux crossing the exobase is larger than the escaping flux. Therefore a large proportion of the carbon atoms produced in dissociation of the CO_2 and CO molecules indeed escape the planet.

[39] From the present calculations the cumulated nonthermal escape rates of atomic oxygen due to sputtering and dissociative recombination are 2.15×10^{25} and 8.7×10^{25} s^{-1} at low and high solar activities, respectively. These rates can be compared to other nonthermal sources of atmospheric escape, including ion escape and ionospheric

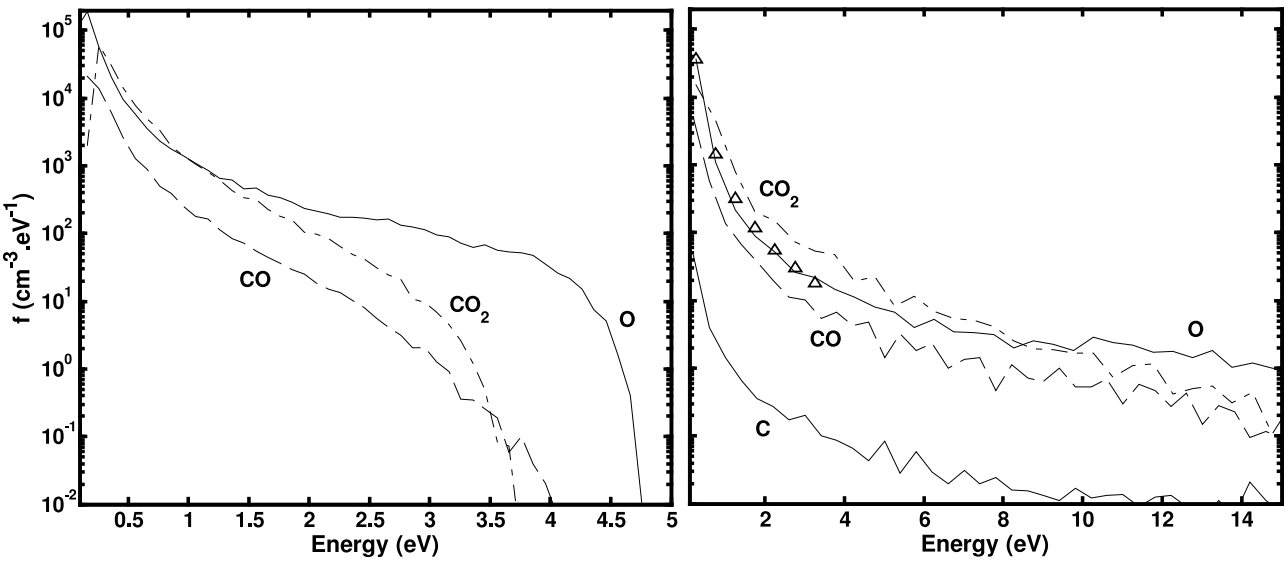

Figure 5. Energy distribution of hot atoms and molecules created by sputtering (right side) and dissociative recombination (left side) at 200 km at high solar activity. The energy thresholds below which hot particles are not considered are 0.082 eV for O, 0.225 eV for CO_2, 0.143 eV for CO, and 0.061 eV for C. The triangled line shows a variation of the oxygen profile as a $\propto E^{-2.9}$ power law at low energies in the case of sputtering.

outflow. Results from ASPERA measurements [*Lundin et al.*, 1989] at high solar activity indicate a global escape rate of oxygen O^+ (dominating) and O_2^+ ions of 3×10^{25} s^{-1}. Results from TAUS instrument indicates an O^+ flux in the plasma sheet an order of magnitude lower. Ion escape and ionospheric outflow have recently been investigated by studying the direct interaction of the solar wind with the planet through a multifluid MHD model by *Ma et al.* [2004] and the hybrid MHD model if the work of *Modolo et al.* [2005]. The oxygen ion escape rate deduced by *Ma et al.* [2004] is in the ranges of $0.54-2.2 \times 10^{24}$ to $2.3-2.8 \times 10^{24}$ s^{-1} at low and high solar activities. In the case of the work of *Modolo et al.* [2005] a range of $0.57-2.44 \times 10^{24}$ s^{-1} for low and high solar activities has been calculated. Both results are less than ASPERA measurements by about one order on magnitude, and therefore more consistent with TAUS results. The same estimation using a test particle code of *Lammer et al.* [2003] for solar average conditions (1EUV) gives an escape flux of 3×10^{24} s^{-1}. These numbers, compared to our results, tend therefore to indicate that ion escape and ionospheric outflow are less efficient escape mechanisms than sputtering at high solar activity and than dissociative recombination at both low and high solar activities. The major escape of the Martian atmosphere thus seems to be in the neutral form rather than in an ionized form.

3.3. Energy and Velocity Distributions

[40] Hot atomic and molecular energy distributions calculated at high solar activity at 200 km can be seen in Figure 5 for DR (left panel) and sputtering (right panel). The energy is limited to the range 0–15 eV where the distribution densities are the largest.

[41] The energy distribution of hot O resulting from collisions with O produced in the DR of O_2^+ (solid line) is similar in shape than in the work of *Krestyanikova and Shematovich* [2005]. The sharp decreasing of this distribution for energies larger than 5 eV clearly differentiate DR from sputtering as a source of hot O in the exosphere. We can mention that, on Earth, various nonthermal sources of hot oxygen have been thought to contribute to the heating of the upper atmosphere and to the geocoronal density [*Gerard et al.*, 1995]. If active at Mars, those sources could influence the shape of the energy distribution that we have derived. In particular, hot thermospheric O(^{3}P) atoms can be created in quenching cooling of O(^{1}D) atoms, which are a major product of DR of O_2^+. This reaction has an exothermicity of 1.96 eV [see, e.g., *Kharchenko et al.*, 2005] and is therefore of interest at Mars. However, on Earth, atomic oxygen becomes the major thermospheric component above roughly 150 km, that is, well below the exobase, whereas, at Mars, atomic O density becomes larger than CO_2 density essentially above the exobase. Therefore full numerical modeling of this source at Mars is required in order to quantify its efficiency at producing an additional hot O exospheric population.

[42] In the terminology used by *Johnson* [1990], a recoil particle is a hot atom or molecule of the atmosphere whose translational energy is gained during a collision cascade initiated by an incident energetic ion or neutral. Such a collision cascade results in an increasing number of recoils with decreasing energy. The energy distribution of the recoils can be described by a Maxwell-Boltzmann distribution at the exobase temperature T_{ex} with an energetic tail. For suprathermal recoils created through collisions with a primary recoil of energy E_i, this energy tail takes the form [e.g., *Johnson*, 1990, 1994]

$$f(E) \approx \beta E_i / E^2 \, E_i > E \gg kT_{ex} \tag{5}$$

where E is the "secondary" recoil particle energy and β a factor depending on the incident ion angle, energy, and

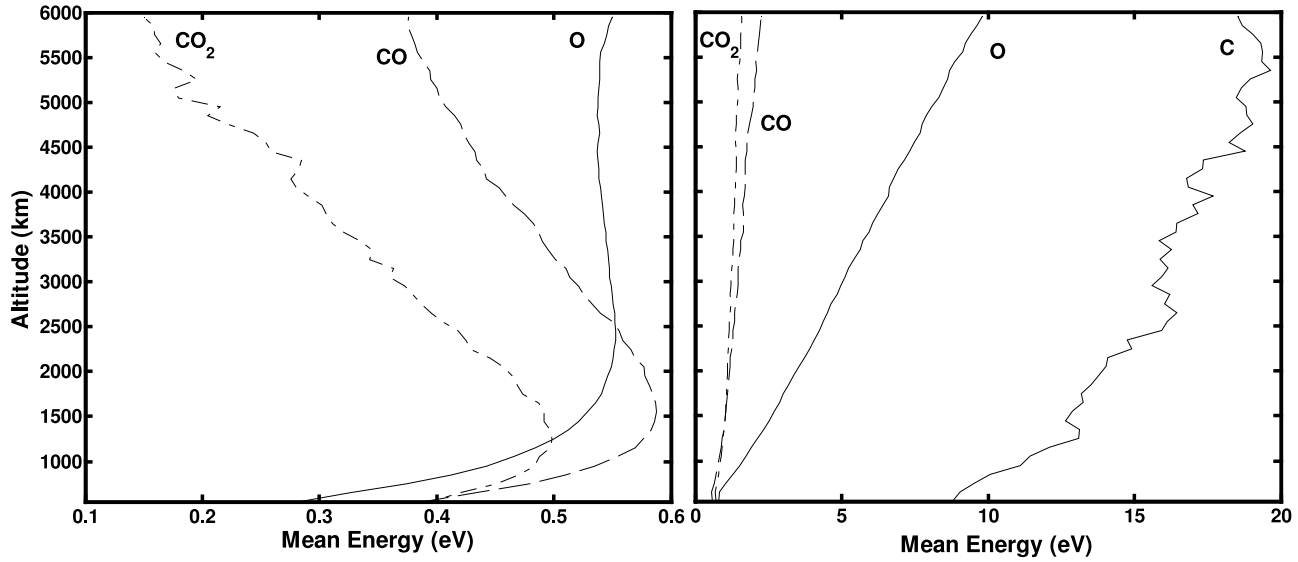

Figure 6. Mean energy profiles for hot O, C, CO, and CO_2 calculated at high solar activity in the case of dissociative recombination of O_2^+ (left side) and sputtering (right side). The plots are valid above 375 km in altitude.

collision cross section ($\beta \approx 1$ in the case of hard sphere collision [*Johnson*, 1994]).

[43] The hot oxygen energy distributions associated to DR and sputtering that we have computed (solid lines in Figure 5) actually have a different energy decrease. Polynomial fits of the energy distributions yield a decrease following $\propto E^{-2.9}$ in the case of sputtering and $\propto E^{-2.4}$ in the case of DR.

[44] In the case of DR, the mean energy of the atoms produced in DR of O_2^+ being equal to 2.3 eV, we have carried out the same fit for energies above 1 eV such that the condition $E_i > E$ of equation (5) holds for 95% of the hot O produced. In that portion of the energy distribution, the best fit is by a $\propto E^{-2.1}$ power law, which is then very close to the recoil distribution predicted by *Johnson* [1990].

[45] In order to understand the observed behavior in the case of sputtering, a first test was carried out by considering the case of a fully dissociated atmosphere composed of oxygen atoms. Collisions are essentially described with the use of a universal potential. The energy distribution of the hot oxygen at 200 km was then found to closely decay as $\propto E^{-2}$. In addition, in a Monte Carlo study of the sputtering of SO_2 molecules from the Io atmosphere by *Pospieszalska and Johnson* [1996], the authors observed an energetic decay close to $\propto E^{-2}$. In this study the molecules were treated as entities having no internal structure and interacting following the Hard Sphere approximation (dissociations were ignored). At last a second test was then carried out by turning off dissociations in our simulation. This resulted again in a decay law very close to relation equation (5). Because of sputtering, which is a more energetic process than DR, we have seen that the hot atomic oxygen population is in a significant proportion issued from molecular dissociations. We therefore conclude that this is because we have a large proportion of hot O atoms created from dissociations of CO_2 and CO molecules that the energy distribution slightly differ from the theoretical energy distribution associated with collision cascade as described in the work of *Johnson* [1990]. This feature interestingly turns out as another signature in the exosphere that could be used to distinguish sputtering products from DR products.

[46] Integration of the hot carbon energy distribution (dotted line) for energies larger than the escape threshold of 1.48 eV shows that, because of sputtering, about 57% of the hot carbon component originating in CO_2 molecules escape from the atmosphere. In the case of CO_2 (dotted-dashed line), this fraction falls to a value lower than 0.5%. This is consistent with the arrangement of the density profiles of atomic carbon and CO_2 observed on Figure 3, as explained in section 3.1. At high solar activity we notice that the maximum energy densities for hot O produced in both processes are of the same order (we find 3.6×10^4 cm^{-3} ev^{-1} at 0.26 eV in the case of sputtering, whereas, in the case of dissociative recombination, we have 5.7×10^4 cm^{-3} ev^{-1}). Figure 6 displays the calculated mean energy profiles of the hot population produced in sputtering and DR of O_2^+, as a function of altitude, and at high solar activity. The profiles of the hot molecules created in collisions with hot O produced in DR of O_2^+ (dashed and dotted-dashed lines) reach their maxima in a range extending from 0.5 to 0.6 eV between 1000 and 1500 km, where the kinetic energy coming from the momentum transfer is exceeded by the gravitational potential energy. The comparatively very large calculated mean energy of the sputtered products are consistent with the results from the work of *Leblanc and Johnson* [2001].

[47] Figure 7 shows the velocity distributions of the hot atomic oxygen and carbon in the phase space at high solar activity produced by sputtering (right side), by DR of O_2^+ (left side of Figure 7a), and by DR of CO^+ (left side of Figure 7c) at 1000 km above the Martian surface. The distributions are plotted in the (radial, tangential) plane.

[48] We compare our results to the theory of *Chamberlain* [1978] which differentiates classes of exospheric particles in the collisionless approximation, depending on the nature of

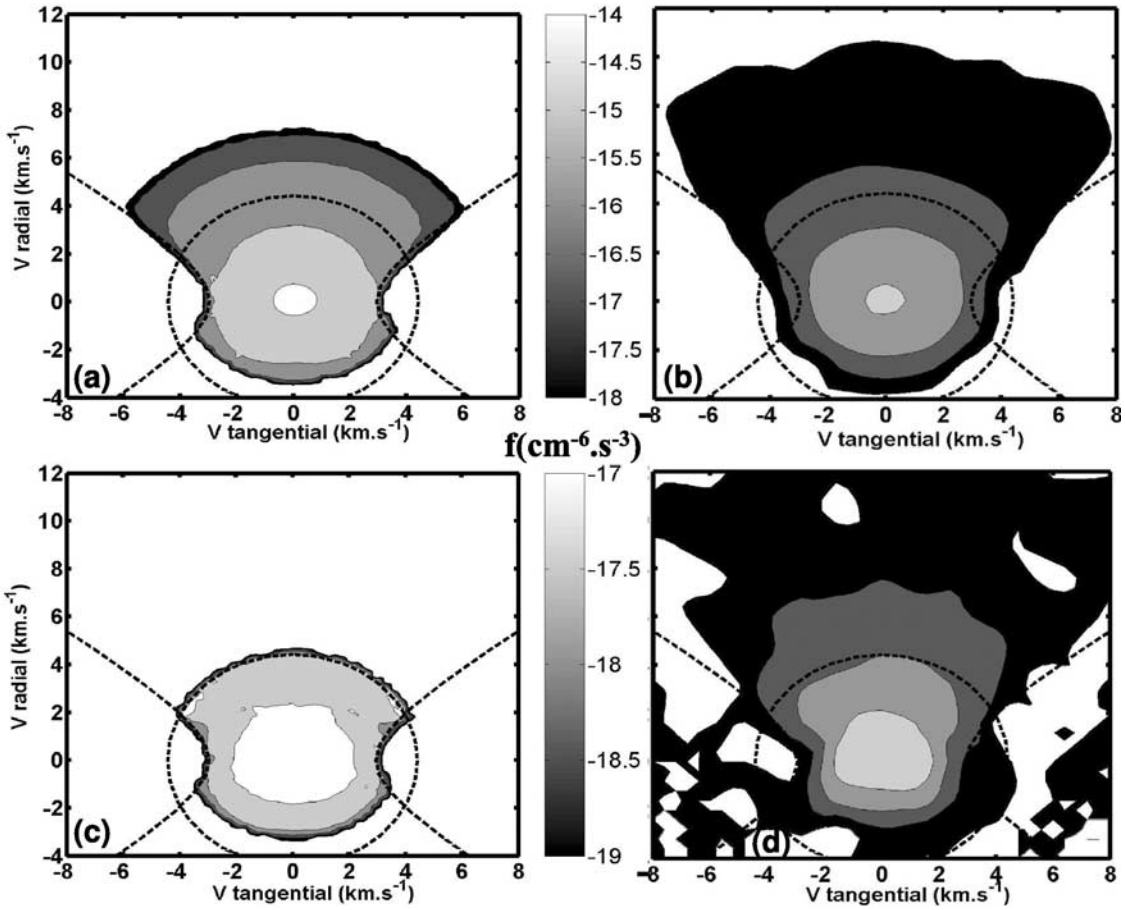

Figure 7. Velocity distributions for hot O and C at 1000 km above the surface created by sputtering (right side) and dissociative recombination reactions (left side) in the phase space as a function of the radial and tangential velocity components. The mean radial velocities are equal to 0.31 and 0.54 km s^{-1} in the case of oxygen on Figures 7a and 7b plots and 0.11 and 0.59 km s^{-1} in the case of carbon on Figures 7c and 7d plots, respectively. In the case of oxygen the inner/outer contour values are fixed at 10^{-14} cm^{-6} s^{-3}/10^{-18} cm^{-6} s^{-3}. In the case of carbon those are fixed at 10^{-17} cm^{-6} s^{-3}/10^{-19} cm^{-6} s^{-3}.

their trajectories. Escaping atoms having Vr > 0 are located in the area between the hyperbola and outside the dashed circle whose radius is equal to the escape velocity at the altitude considered. The area inside the circle and outside the two dashed hyperbola is theoretically populated by satellites particles, which never cross the critical level of the exobase (in our case located near 225 km for O at high solar activity). Such particles are present in the case of sputtering and may result from collisions above the theoretical exobase leading to an enhancement of the polar or azimuthal velocity components, which thus behave as long-term satellites particles. In the case of carbon for which the densities are low, some numerical noise also occurs in this area. The phase space density is indeed about 2 orders of magnitude lower for carbon than it is in the case of oxygen. The shape of the velocity distribution for hot O atoms calculated in the case of DR is in good agreement with that obtained in the work of *Hodges* [2000] (except for the tangential shift due to the effect of corotation in the work of *Hodges* [2000]). The outermost isodensity line corresponding to 10^{-16} cm^{-6} s^{-1} is close to Vr = 6 km s^{-1} for Vt = 0 in our case.

[49] Both DR and sputtering produce an upward flux of escaping oxygen atoms. In the case of sputtering, this flux appears as more extended along the radial direction. Hence the angular spreading of this flux should be narrower than that of the flux due to DR. As already mentioned, DR of CO^+ is not responsible for a significant flux of escaping carbon. In contrast, sputtering produces hot carbon with velocities highly elongated in the radial direction (even compared to the case of hot oxygen). In the case of dissociative recombination, the shape of the velocity distributions clearly reflects the presence of escaping particles and the lack of satellites, a result that was also obtained in the equatorial plane by *Hodges* [2000] with a three-dimensional Monte-Carlo model in the Mars-L case.

4. Conclusion

[50] A numerical scheme based on a Monte Carlo approach coupled with a molecular dynamic model is used to describe

the hot neutral component of the Martian corona created by both sputtering and dissociative recombination reactions of O_2^+ and CO^+ ions as a function of the solar activity. The species described are hot atomic O and C, as well as hot molecular CO and CO_2. Density profiles, energy and velocity distributions, as well as escape rates, have been derived at low and high solar activities for both processes.

[51] At high solar activity, sputtering is seen to significantly contribute to the hot corona. Indeed, the sputtered hot oxygen density is only a factor of 1.6 lower than the hot O density due to DR at 1000 km. The oxygen escape rate due to sputtering represents 75% of the rate due to DR of O_2^+. Because of sputtering, CO and CO_2 molecules are also predicted to efficiently populate the corona. The loss rate of carbon (in all forms) induced by sputtering is larger than the rate due to photochemical sources as calculated in the studies of *Nagy et al.* [2001] and *Fox* [2004]. Because of its small escape energy and the low gravity field of the planet, about 60% of the sputtered carbon atoms produced by dissociations of the CO_2 molecules by incident pick-up ions escape from the atmosphere at high solar activity. The escape rate of such atomic carbon is comparable to the escape rate of carbon created by photodissociation of CO as calculated by *Nagy et al.* [2001]. At both high and low solar activities, collisions of hot O created in DR of O_2^+ with the atmospheric background also produces hot CO and CO_2 exospheric populations. We have observed that the density profiles of hot exospheric CO_2 exhibit different scale heights depending on the nonthermal source.

[52] Cumulated escape rates of the nonthermal mechanism are estimated to 2.15×10^{25} and 8.7×10^{25} s^{-1} at low and high solar activity, respectively. Comparison of our rates with those from others authors tend to indicate that sputtering is a more efficient escape mechanism than ionic escape and ionospheric outflow at high solar activity. DR of O_2^+ also dominates the escape at both low and high solar activities. The hot oxygen energy spectra associated with sputtering and DR of O_2^+ ions near the exobase are found to closely decay as E^{-3} and E^{-2}, respectively.

[53] Several factors will actually influence our results. The O_2^+ density is known to vary as a function of the SZA [see, e.g., *Zhang et al.*, 1990]. It is also known to be sensitive to seasonal effects because of the stronger solar radiation at perihelion due to the Martian orbit eccentricity. Dust storms also affect the global thermospheric dynamics and ionospheric peak altitude (because of absorption of solar energy by dust particles) [*Bougher and Shinagawa*, 1998]. Thermospheric tidal and gravity waves [*Forbes et al.*, 2001] trigger thermospheric temperature variations. *Bougher et al.* [2004] presented evidence for stable longitudinal variation of the ionosphere peak height at high latitudes at the aphelion from the observations of an interannual variability of the MGS radio science electron density profiles. Such an effect may have a strong signature in the hot O corona produced by DR of O_2^+ as suggested in this work. Other effects can be assigned to crustal magnetic anomalies that drives minimagnetospheric structures (<400 km) able either to trap and heat electrons or to reconnect with the IMF, allowing the solar wind particles to interact directly with the atmosphere, especially in the southern hemisphere [*Breus et al.*, 2004; *Bertaux et al.*, 2005; *Krymskii et al.*, 2003]. Recent hybrid MHD simulation by *Modolo et al.* [2005] shows strong asymmetry of the plasma distribution around Mars, depending on the convection electric field direction. In particular, it will influence the creation of O^+ pick-up ions and the variation of their impact location on the atmosphere [*Modolo et al.*, 2004]. Effects of coronal mass ejection events on the thermosphere/ionosphere system are still poorly documented and studied but also have to be taken into account [*Leblanc et al.*, 2002; *Brain et al.*, 2004]. Of particular importance is the potential feedback due to atmospheric inflation induced by sputtering [see *Johnson and Luhmann*, 1998]. At last the effect of energetic O_2^+ ions impacting the atmosphere (that may compete with the O^+ pick-up ion flux) should also be investigated through simulation.

[54] The sputtered escape rates calculated here, combined with other estimates of photochemical carbon escape rates at high solar activity, show that the total carbon escape rate remains in the range of 1 to 2×10^{25} s^{-1}, which corresponds to a ratio of 30 to 10% of the photochemical escape rate of oxygen. The sputtered oxygen escape rate, as well as that of carbon in all forms, is expected to have been greatly enhanced in the ancient solar system, when the EUV solar flux was much stronger. The atmospheric depletion since 3.5 Gyr from those nonthermal processes is a key question to be addressed to understand the planet's history and the possibility of an early wet environment conducive to the emergence of life. Current evolutionary models of the Martian atmosphere and solar wind parameters suffer from the lack of constraints on the involved escaping fluxes and processes, stressing the necessity of measurements of the hot neutral population in a future mission to Mars. The main goals of such a measurement would be to constrain the value of the upwelling fluxes created in DR and sputtering. From our results at 400-km altitude this fluxes are predicted to be a mixture of hot O, CO_2, CO, and C in respective proportion (0.88, 0.07, 0.05, 0.0) in the case of DR and (0.27, 0.42, 0.3, 0.01) in the case of sputtering. The radial elongation of the velocity distributions plotted in Figure 7 imply that a wide instrumental field of view should not be necessary. The measurement of the three-dimensional hot coronal structure, as a function of the solar wind intensity and thermospheric/ionospheric parameters, should greatly help us to understand Mars interaction with the solar wind. These objectives can be partly achieved by measuring the energy spectra of the low-energy neutral exospheric particles, as well as by comparing the fluxes at different locations around Mars. In order to carry out such measurements the pericenter of the satellite should be significantly below 300 km. A mass separation mode would also be required in order to detect the contribution of heavy species to the coronal structure. The different density scale heights observed in our simulation in the case of hot CO_2 can also serve as a useful criteria to differentiate DR and sputtering processes.

[55] **Acknowledgments.** The authors acknowledge the referees, particularly one of them, for their in-depth reading of the paper and their help in clarifying the first version. Many thanks also go to R.E. Johnson and V. Shematovich for their useful comments on the submitted work. This work makes use of results produced by the Enabling Grids for E-sciencE project, a project cofunded by the European Commission (under contract INFSO-RI-031688) through the Sixth Framework Programme. Full information is available at http://www.eu-egee.org. Thanks to David Weissenbach

(IPSL) and the Institute of Informatics of the Academia of Slovakia (UISAV) for their help to port the application on EGEE.

References

Alge, E., N. G. Adams, and D. Smith (1983), Measurements of the dissociative recombination coefficients of O_2^+, NO^+, and $NH4^+$ in the temperature range 200–600 K, *J. Phys. B*, *16*, 1433–1444.

Allen, M. P., and D. J. Tildesley (1987), Computer Simulation of Liquids, Clarendon Press, Oxford.

Anderson, D. E., and C. W. Hord (1971), Mariner 6 and 7 ultraviolet spectrometer experiment: Analysis of hydrogen Lyman alpha data, *J. Geophys. Res.*, *76*, 6666–6673.

Bertaux, J.-L., F. Leblanc, O. Witasse, E. Quemerais, J. Lilensten, S. A. Stern, B. Sandel, and O. Korablev (2005), Discovery of an aurora on Mars, *Nature*, *435*, 790–794.

Bougher, S. W., and H. Shinagawa (1998), The Mars thermosphere-ionosphere: Predictions for the arrival of Planet-B, *Earth Planets Space*, *50*, 247–257.

Bougher, S. W., S. Engel, D. P. Hinson, and J. R. Murphy (2004), MGS Radio Science electron density profiles: Interannual variability and implications for the Martian neutral atmosphere, *J. Geophys. Res.*, *109*(E18), E03010, doi:10.1029/2003JE002154

Brain, D. A., F. Leblanc, J. G. Luhmann, G. T. Delory, R. A. Mewaldt, and C. M. Cohen (2004), Effects of Solar Energetic Particle Events on the Martian Surface and Atmosphere, AGU, Fall Meeting, Abstracts SH53C-04, pp. C4+.

Brecht, S. H. (1997), Hybrid simulations of the magnetic topology of Mars, *J. Geophys. Res.*, *102*(11), 4743–4750, doi:10.1029/96JA03205.

Breus, T. K., A. M. Krymskii, D. H. Crider, N. F. Ness, D. Hinson, and K. K. Barashyan (2004), Effect of the solar radiation in the topside atmosphere/ionosphere of Mars: Mars Global Surveyor observations, *J. Geophys. Res.*, *109*(A18), A09310, doi:10.1029/2004JA010431.

Carlsson, E., A. Fedorov, S. Barabash, E. Budnik, A. Grigoriev, H. Gunell, H. Nilsson, and J.-A. Sauvaud, et al. (2006), Mass composition of the escaping plasma at Mars, *Icarus*, *182*, 320–328, doi:10.1016/j.icarus.2005.09.020.

Chamberlain, J. W. (1978), *Theory of Planetary Atmosphere*, Elsevier, New York.

Chassefière, E., F. Leblanc, and B. Langlais (2006), The combined effects of escape and magnetic field histories at Mars, *Planet. Space Sci.*, *55*, 343–357.

Forbes, J. M., M. E. Hagan, S. W. Bougher, and J. L. Hollingsworth (2001), Kelvin wave propagation in the upper atmospheres of Mars and Earth, *Adv. Space Res.*, *27*, 1791–1800.

Fox, J. L. (1993), On the escape of oxygen and hydrogen from Mars, *Geophys. Res. Lett.*, *20*, 1747–1750.

Fox, J. L. (2004), CO_2^+ dissociative recombination: A source of thermal and nonthermal C on Mars, *J. Geophys. Res.*, *109*(A18), A08306, doi:10.1029/2004JA010514.

Fox, J. L., and F. M. Bakalian (2001), Photochemical escape of atomic carbon from Mars, *J. Geophys. Res.*, *106*, 28,785–28,796, doi:10.1029/2001JA000108.

Fox, J. L., and A. Hać (1997a), Spectrum of hot O at the exobases of the terrestrial planets, *J. Geophys. Res.*, *102*(11), 24,005–24,012.

Fox, J. L., and A. Hać (1997b), The 15N/14N isotope fractionation in dissociative recombination of N_2^+, *J. Geophys. Res.*, *102*(11), 9191–9204, doi:10.1029/97JE00086.

Fox, J. L., and A. Hać (1999), Velocity distributions of C atoms in CO^+ dissociative recombination: Implications for photochemical escape of C from Mars, *J. Geophys. Res.*, *104*(13), 24,729–24,738, doi:10.1029/1999JA900330.

Gerard, J. C., P. G. Richards, V. I. Shematovich, and D. V. Bisikalo (1995), The importance of new chemical sources for the hot oxygen geocorona, *Geophys. Res. Lett.*, *22*, 279–282.

Hanson, W. B., S. Sanatani, and D. R. Zuccaro (1977), The Martian ionosphere as observed by the Viking retarding potential analyzers, *J. Geophys. Res.*, *82*(11), 4351–4363.

Hodges, R. R. (2000), Distributions of hot oxygen for venus and mars, *J. Geophys. Res.*, *105*.

Hodges, R. R. (2002), The rate of loss of water from Mars, *Geophys. Res. Lett.*, *29*(3), 1038, doi:10.1029/2001GL013893.

Johnson, R. E. (1990), *Energetic Charged-Particle Interactions with Atmospheres and Surfaces*, Springer, New York, also Physics and Chemistry in Space, volume 19.

Johnson, R. E. (1994), Plasma-induced sputtering of an atmosphere, *Space Sci. Rev.*, *69*, 215–253.

Johnson, R. E., and M. Liu (1998), Sputtering of the atmosphere of Mars: I. Collisional dissociation of CO_2, *J. Geophys. Res.*, *103*(12), 3639.

Johnson, R. E., and J. G. Luhmann (1998), Sputter contribution to the atmospheric corona on Mars, *J. Geophys. Res.*, *103*(12), 3649.

Johnson, R. E., D. Schnellenberger, and M. C. Wong (2000), The sputtering of an oxygen thermosphere by energetic O^+, *J. Geophys. Res.*, *105*(14), 1659–1670, doi:10.1029/1999JE001058.

Kabin, K., and B. D. Shizgal (2002), Velocity distributions of energetic atoms in planetary exospheres from dissociative recombination, *J. Geophys. Res.*, *107*(E7), 5053, doi:10.1029/2000JE001479.

Kella, D., P. J. Johnson, H. B. Pedersen, L. Vejby-Christensen, and L. H. Andersen (1997), The source of green light emission determined from a heavy-ion storage ring experiment, *Science*, *276*, 1530–1533.

Kharchenko, V., A. Dalgarno, B. Zygelman, and J.-H. Yee (2000), Energy transfer in collisions of oxygen atoms in the terrestrial atmosphere, *J. Geophys. Res.*, *105*(14), 24,899–24,906, doi:10.1029/2000JA000085.

Kharchenko, V., A. Dalgarno, and J. L. Fox (2005), Thermospheric distribution of fast O(1D) atoms, *J. Geophys. Res.*, *110*(A9), A12305, doi:10.1029/2005JA011232.

Kim, J., A. F. Nagy, J. L. Fox, and T. E. Cravens (1998), Solar cycle variability of hot oxygen atoms at Mars, *J. Geophys. Res.*, *103*(12), 29,339–29,342.

Krasnopolsky, V. A. (2002), Mars' upper atmosphere and ionosphere at low, medium, and high solar activities: Implications for evolution of water, *J. Geophys. Res.*, *107*(E12), 5128, doi:10.1029/2001JE001809.

Krasnopolsky, V. A., and P. D. Feldman (2001), Detection of molecular hydrogen in the atmosphere of Mars, *Science*, *294*, 1914–1917, doi:10.1126/science.1065569.

Krasnopolsky, V. A., M. J. Mumma, and G. Randall Gladstone (1998), Detection of atomic deuterium in the upper atmosphere of Mars, *Science*, *280*, 1576.

Krestyanikova, M. A., and V. I. Shematovich (2005), Stochastic models of hot planetary and satellite coronas: A photochemical source of hot oxygen in the upper atmosphere of Mars, *Sol. Syst. Res.*, *39*, 22–32, doi:10.1007/s11208-005-0012-7.

Krymskii, A. M., T. K. Breus, N. F. Ness, D. P. Hinson, and D. I. Bojkov (2003), Effect of crustal magnetic fields on the near terminator ionosphere at Mars: Comparison of in situ magnetic field measurements with the data of radio science experiments on board Mars Global Surveyor, *J. Geophys. Res.*, *108*(A12), 1431, doi:10.1029/2002JA009662.

Lammer, H., H. I. M. Lichtenegger, C. Kolb, I. Ribas, E. F. Guinan, R. Abart, and S. J. Bauer (2003), Loss of water from Mars: Implications for the oxidation of the soil, *Icarus*, *165*, 9–25.

Leblanc, F., and R. E. Johnson (2001), Sputtering of the Martian atmosphere by solar wind pick-up ions, *Planet. Space Sci.*, *49*, 645–656.

Leblanc, F., and R. E. Johnson (2002), Role of molecular species in pickup ion sputtering of the Martian atmosphere, *J. Geophys. Res.*, *107*(E2), 5010, doi:10.1029/2000JE001473.

Leblanc, F., J. G. Luhmann, R. E. Johnson, and E. Chassefiere (2002), Some expected impacts of a solar energetic particle event at Mars, *J. Geophys. Res.*, *107*(A5), 1058, doi:10.1029/2001JA900178.

Luhmann, J. G., and J. U. Kozyra (1991), Dayside pickup oxygen ion precipitation at Venus and Mars—Spatial distributions, energy deposition and consequences, *J. Geophys. Res*, *96*(15), 5457–5467.

Luhmann, J. G., R. E. Johnson, and M. H. G. Zhang (1992), Evolutionary impact of sputtering of the Martian atmosphere by O(+) pickup ions, *J. Geophys. Res.*, *19*, 2151–2154.

Lundin, R., H. Borg, B. Hultqvist, A. Zakharov, and R. Pellinen (1989), First measurements of the ionospheric plasma escape from Mars, *Nature*, *341*, 609–612.

Lundin, R., et al. (2004), Solar wind-induced atmospheric erosion at Mars: First results from ASPERA-3 on Mars Express, *Science*, *305*, 1933–1936, doi:10.1126/science.1101860.

Ma, Y., A. F. Nagy, I. V. Sokolov, and K. C. Hansen (2004), Three-dimensional, multispecies, high spatial resolution MHD studies of the solar wind interaction with Mars, *J. Geophys. Res.*, *109*(A18), D15515, doi:10.1029/2003JA010367.

Mehr, F. J., and M. A. Biondi (1969), Electron temperature dependence of recombination of O_2^+ and N_2^+ ions with electrons, *Phys. Rev.*, *181*, 264–27110.1103/PhysRev.181.264.

Modolo, R., J.-Y. Chaufray, F. Leblanc, and G. Chanteur (2004), Impacting flux and associated sputtering effects at Mars, in 35th COSPAR Scientific Assembly, p. 3018.

Modolo, R., G. M. Chanteur, E. Dubinin, and A. P. Matthews (2005), Influence of the solar EUV flux on the Martian plasma environment, *Ann. Geophys.*, *23*, 433–444.

Nagy, A. F., and P. M. Banks (1970), Photoelectron fluxes in the ionosphere, *J. Geophys. Res.*, *75*, 6260–6270.

Nagy, A. F., M. W. Liemohn, J. L. Fox, and J. Kim (2001), Hot carbon densities in the exosphere of Mars, *J. Geophys. Res.*, *106*(15), 21,565–21,568, doi:10.1029/2001JA000007.

Petrignani, A., W. J. van der Zande, P. C. Cosby, F. Hellberg, R. D. Thomas, and M. Larsson (2005), Vibrationally resolved rate coefficients and

branching fractions in the dissociative recombination of O_2^+, *J. Chem. Phys.*, *122*, 014,302.

Peverall, R., et al. (2001), Dissociative recombination and excitation of O_2^+: Cross sections, products yields and implications for studies of ionospheric airglows, *J. Chem. Phys.*, *114*(15), 6679.

Pospieszalska, M. K., and R. E. Johnson (1996), Monte Carlo calculations of plasma ion-induced sputtering of an atmosphere: SO2 ejected from Io, *J. Geophys. Res.*, *101*, 7565–7574, doi:10.1029/95JE03650.

Rohrbaugh, R. P., J. S. Nisbet, E. Bleuler, and J. R. Herman (1979), The effect of energetically produced O_2^+ on the ion temperatures of the Martian thermosphere, *J. Geophys. Res.*, *84*, 3327–3338.

Rosen, S., R. Peverall, and M. Larsson, et al. (1998), Absolute cross sections and final-state distributions for dissociative recombination and excitation of CO^+, using an ion storage ring, *Phys. Rev. A*, *57*, 4462–4470.

Schunk, R. W., and A. F. Nagy (2000), *Ionospheres*, Cambridge Univ. Press, New York.

Sheehan, C. H., and J. P. St-Maurice (2004), Dissociative recombination of N_2^+, O_2^+, and NO^+: Rate coefficients for ground state and vibrationnaly excited ions, *J. Geophys. Res.*, *109*, A03302, doi:10.1029/2003JA010132.

Shematovich, V. I. (2004), Stochastic models of hot planetary and satellite coronas, *Sol. Syst. Res.*, *38*, 28–38, doi:10.1023/B:SOLS.0000015153.66874.25.

Shematovich, V., J. Gérard, D. V. Bisikalo, and B. Hubert (1999), Thermalization of O1D atoms in the thermosphere, *J. Geophys. Res.*, *104*(13), 4287–4296, doi:10.1029/1998JA900154.

Spreiter, J. R., and S. S. Stahara (1980), A new predictive model for determining solar wind-terrestrial planet interactions, *J. Geophys. Res.*, *85*(14), 6769–6777.

Tully, C., and R. E. Johnson (2001), Low energy collisions between ground-state oxygen atoms, *Planet. Space Sci.*, *49*, 533–537.

Zhang, M. H. G., J. G. Luhmann, and A. J. Kliore (1990), An observational study of the nightside ionospheres of Mars and Venus with radio occultation methods, *J. Geophys. Res.*, *95*(14), 17,095–17,102.

Zhang, M. H. G., J. G. Luhmann, S. W. Bougher, and A. F. Nagy (1993), The ancient oxygen exosphere of Mars—Implications for atmosphere evolution, *J. Geophys. Res.*, *98*(17), 10,915.

Ziegler, J. F., J. P. Biersack, and U. Littmark (1985), The Stopping and Range of Ions in Solids, The Stopping and Range of Ions in Matter, Elsevier, New York.

J. J. Berthelier and F. Cipriani, Centre d'Etude des Environnements Terrestres et Planétaires/IPSL, Saint-Maur, France. (fabrice.cipriani@cetp.ipsl.fr)

F. Leblanc, Service d'Aronomie du CNRS/IPSL, Verrières-Le-Buisson, France.